Renewable and Sustainable Energy Reviews 111 (2019) 261–275

Contents lists available at ScienceDirect

Renewable and Sustainable Energy Reviews

journal homepage: www.elsevier.com/locate/rser

Meteorological conditions leading to extreme low variable renewable energy production and extreme high energy shortfall

K. van der Wiel[a,*], L.P. Stoop[a,b], B.R.H. van Zuijlen[c], R. Blackport[d], M.A. van den Broek[c], F.M. Selten[a]

[a] Royal Netherlands Meteorological Institute, De Bilt, the Netherlands
[b] Institute for Marine and Atmospheric Research, Utrecht University, Utrecht, the Netherlands
[c] Copernicus Institute of Sustainable Development, Utrecht University, Utrecht, the Netherlands
[d] College of Engineering, Mathematics and Physical Sciences, University of Exeter, Exeter, United Kingdom

ARTICLE INFO

Keywords:
Variable renewable energy
Energy transition
Energy security
Extreme weather
Energy meteorology
Climate change
Climate impacts

ABSTRACT

To mitigate climate change a renewable energy transition is needed. Existing power systems will need to be redesigned to balance variable renewable energy production with variable energy demand. We investigate the meteorological sensitivity of a highly-renewable European energy system using large ensemble simulations from two global climate models. Based on 3×2000 years of simulated weather conditions, daily wind and solar energy yields, and energy demand are calculated. From this data, 1-, 7- and 14-days events of extreme low renewable energy production and extreme high energy shortfall are selected. Energy shortfall is defined as the residual load, i.e. demand minus renewable production. 1-day low energy production days are characterised by large-scale high pressure systems over central Europe, with lower than normal wind speeds. These events typically occur in winter when solar energy is limited due to short day lengths. Situations of atmospheric blocking lead to long lasting periods of low energy production, such 7- and 14-days low production events peak late summer. High energy shortfall events occur due to comparable high pressure systems though now combined with below normal temperatures, driving up energy demand. In contrast to the low energy production events, 1-, 7- and 14-days high shortfall events all occur mid-winter, locked to the coldest months of the year. A spatial redistribution of wind turbines and solar panels cannot prevent these high-impact events, options to import renewable energy from remote locations during these events are limited. Projected changes due to climate change are substantially smaller than interannual variability. Future power systems with large penetration of variable renewable energy must be designed with these events in mind.

1. Introduction

To mitigate future climate change a decarbonisation of global society is needed [1,2]. The transition from carbon-intensive fossil fuels to low- or zero-carbon renewable energy sources, in combination with energy saving measures and increased energy efficiency [3], will help achieve net zero emissions [4] and limit dangerous climate change impacts [5–9]. The fact that energy production from most renewable energy sources, most notably wind and solar electricity production, depends strongly on meteorological conditions complicates this energy transition [10–18]. Temporal meteorological variability leads to temporal variability in the production of renewable energy. This is fundamentally different from the production of energy in a conventional power plant which can be managed in time. Therefore, to guarantee both short and long term energy security, existing power systems will need to be redesigned [3,19].

A big challenge in the design of highly-renewable power systems is how to deal with periods of low energy production [20]. Further complications in the design arise due to the variability of energy demand. Meteorological variability, through the variation of outdoor air temperatures and available light among others, causes part of the variability in energy demand [17,21–26]. Matching variable energy demand and variable renewable energy production, and therewith achieving balance in the power system, is a challenge of high societal importance. The aim of this study is to contribute to this challenge with meteorological insights.

Power systems with high penetrations of wind and solar energy will likely include back-up low or no-carbon power plants (which can

* Corresponding author.
E-mail address: wiel@knmi.nl (K. van der Wiel).

https://doi.org/10.1016/j.rser.2019.04.065
Received 29 November 2018; Received in revised form 22 March 2019; Accepted 23 April 2019

Nomenclature

Abbreviations

CMIP5	Coupled Model Intercomparison Project Phase 5
DJF	December-January-February
ENTSO-E	European Network of Transmission System Operators for Electricity
GEV	Generalized Extreme Value
GMST	Global Mean Surface Temperature
JJA	June-July-August
RCP	Representative Concentration Pathway
SI	Supporting Information
st.dev	Standard deviation

Symbols

α	Roughness parameter
α_1	Model parameter TWh day^{-1}
α_2	Model parameter TWh day^{-1}
β_1	Model parameter TWh day^{-1} °C^{-1}
β_2	Model parameter TWh day^{-1} °C^{-1}
γ	Model parameter
ζ	Model parameter °C^{-1}
c	Model parameter °C
c_1	Model parameter °C
c_2	Model parameter
c_3	Model parameter °C m^2 W^{-1}
c_4	Model parameter °C s m^{-1}
D	Energy demand TWh day^{-1}
E_{pot}	Potential for renewable energy production
F	Model smoothing function
G	Incoming solar radiation W m^{-2}
G_{stc}	Incoming solar radiation under standard test conditions W m^{-2}
h	Hub height m
h_0	Reference height m
IC	Installed capacity TW
P	Energy production TWh day^{-1}
P_R	Performance ratio
PV_{pot}	Potential for renewable solar energy production
r	Correlation coefficient
S	Energy shortfall TWh day^{-1}
t	Time days
$T_{a,day}$	Daytime air temperature °C
$T_{a,mean}$	Mean daily air temperature °C
$T_{a,max}$	Maximum daily air temperatusre °C
T_{cell}	Temperature of a solar cell °C
t_{oper}	Total operational time hours day^{-1}
T_{ref}	Reference temperature °C
V	Wind speed m s^{-1}
V_{ci}	Cut-in wind speed m s^{-1}
V_r	Rated wind speed m s^{-1}
V_{co}	Cut-out wind speed m s^{-1}
W_{pot}	Potential for renewable wind energy production

increase production at short notice), interconnection of electrical grids over large regions (to import renewable energy from remote regions) [27,28], energy storage technologies (which help to move energy from times of abundance to times of shortfall), demand response (the shifting or shedding of electricity demand to make demand match supply), etc. [3,20]. However, these solutions may not be sufficient under extreme conditions. If there is no balance between energy demand and energy production, a power system fails. This leads to power outages, which have significant societal impacts.

In the present paper, the extreme situations that pose a risk for European energy security are identified and the meteorological conditions that cause them are described. The highly-renewable power systems are not yet built, the results can therefore be taken into account in the design efforts. The presented results may help to prevent the failure of the power system under the described conditions, or minimise the occurrence or the consequences of failures. Furthermore, the results open scientific research paths to next investigate the meteorological-based predictability of these events, allowing for better preparation (e.g. using storage technologies, demand response, etc.).

The analysis is based on a large ensemble of meteorological data from two global climate models (EC-Earth, HadGEM2-ES, 3 × 2000 years), for which daily renewable energy production and energy demand are calculated (again 3 × 2000 years, Fig. 1). The exceptional amount of weather data allows for a sampling of extreme events that is not possible based on observational-based data. 1-in-10 year events of high societal impacts are selected based on two energy impact variables: extreme low European renewable energy production and extreme high European energy shortfall. Energy shortfall is defined to be the difference between energy demand and variable renewable energy production, i.e. the residual load. In contrast to a meteorology-centred approach with a focus on extreme weather events, this impact-based method guarantees that only the events with the highest potential impacts are investigated. Here the full distribution of impacts is calculated and no assumptions about the relation between extreme meteorology and extreme societal impacts are made. The weather that leads to 1-in-10 year high-impact events of various length (1-, 7- and 14 days) is described, and changes related to global climate change are briefly discussed.

The remainder of this paper is organised as follows. In Section 2 the

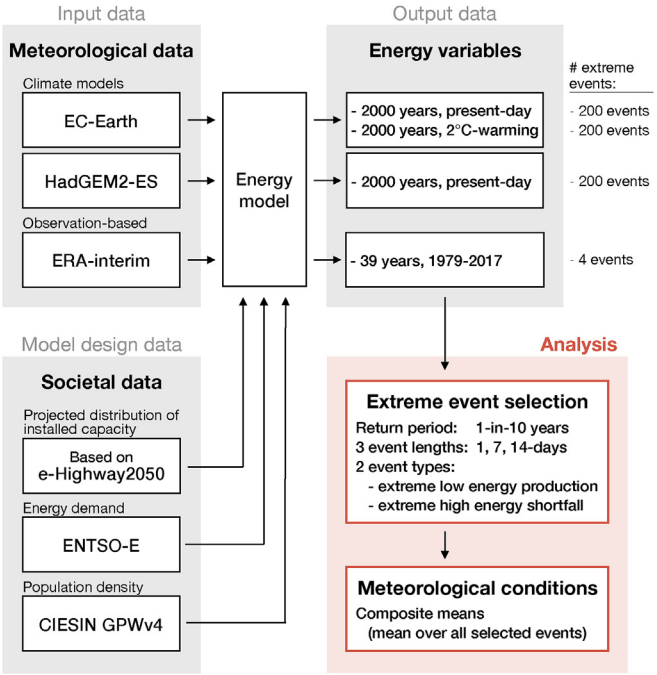

Fig. 1. Flowchart of the study design; more details are provided in the main text (Sections 2 and 3). Meteorological data from two climate models and a re-analysis product are used (top left), combined with societal data (bottom left), these form the input data to an energy model (top centre, Section 3). The resulting energy variables (top right) are analysed, extreme events are selected and meteorological conditions investigated (bottom right).

sequence of modelling steps and the methods used in this study are described. The energy model used to calculate the two energy impact variables of interest is described in Section 3. The results for extreme low renewable energy production events and extreme high energy shortfall events are presented in Sections 4 and 5, respectively. In Section 6 the sensitivity of the results to the global climate model of choice, to the spatial distribution of wind turbines and solar panels and to the effects of climate change is discussed. A discussion of the limitations of this study and its place in the existing literature is provided in Section 7, conclusions are provided in Section 8. Supporting information (SI) with additional figures and observational analysis is available online.

2. Data and methods

A variety of models and data were used to investigate the meteorological conditions giving rise to high risk of European energy security (Fig. 1). The EC-Earth model version 2.3 [29] was used to simulate a large ensemble of weather conditions representing the present-day climate. EC-Earth is a state-of-the-art global coupled climate model, it includes atmospheric, oceanic, land and sea-ice components. The model was used in its CMIP5 configuration, with an atmospheric resolution of approximately 100 km. A description of all individual model components, coupling and the quality of simulated climate variables is provided in Ref. [29].

From sixteen transient climate runs (1861-2100, RCP8.5) the 5-year model period in which the absolute global mean surface temperature (GMST) matched that observed from 2011 to 2015 was selected, observed GMST from HadCRUT4 [30]. Each of the sixteen transient runs were then used as an initial condition for an ensemble of 25 members of five years each, resulting in $16 \times 25 \times 5 = 2000$ years of weather simulations for present-day climate conditions. More information on the large ensemble climate model experiment setup is provided in Ref. [31].

For each day in the climate model simulations the energy impact variables were then calculated, resulting in 2000 years of impact data. The climate model provided daily-averaged variables, the impact variables therefore also represent daily averages. The energy model that was used to make these calculations is described in full detail in Section 3. The potential influence of coarse spatial model resolution and daily-averaged values on our results is discussed in Section 7.

High-impact events were selected from the 2000 years of energy impact data. The events of interest here have an average return period of 10 years, it was assumed that there are 200 such events present in the modelled data. Given the large amount of available data, the analysis did not need to rely on a statistical formulation of the low or high tails of the distribution. Instead extreme events were simulated and sampled, which meant the associated meteorological conditions could be investigated. To describe a typical high-impact event, the mean meteorological conditions (both maps and time series) over the 200 selected events were calculated, these will be referred to as 'composite means'. To investigate events of longer duration, i.e. of 7- and 14-days, running means of the energy impact variables were computed and the selection of events was repeated. To prevent double sampling of essentially the same event (two 7-day events may have six days in common), events were required to be at least three and seven days apart for 7- and 14-days events respectively.

To compare the obtained model results to real-world meteorological conditions, the ERA-interim reanalysis product [32] was used. ERA-interim data is modelled data at approximately 80 km horizontal resolution, boosted in quality by the assimilation of observational data. It describes the historical variability of meteorological conditions. ERA-interim was used to quantify biases in modelled meteorological and energy variables. These biases were not corrected before the analysis. This choice was made to preserve the physical self-consistency of all simulated meteorological variables. Instead, the biases were considered during analysis and their potential influence on the results is discussed in Section 7. The analysis of high-impact events as done for EC-Earth data was repeated using ERA-interim data (figures included in the SI). It is important to note that, because ERA-interim covers only 39 years (1979–2017), the composite means are averages over four events only (approximately 1-in-10 year events). These ERA-interim results are therefore expected to be less robust than the model results, signifying the benefits of the large ensemble model approach.

To investigate the sensitivity of the results to the climate model used, the energy calculations were repeated for a similar 2000 year large ensemble experiment from the HadGEM2-ES global climate model [33] (Section 6.1). To quantify potential effects of climate change, a second 2000 year ensemble from the EC-Earth model was used (Section 6.3). In this ensemble the absolute GMST was chosen to be the pre-industrial temperature plus 2°C global warming, inspired by the climate goal of the Paris agreement [34]. Pre-industrial temperature was defined to be the HadCRUT4 mean over the years 1850–1899.

3. Energy model

An energy model was developed to transform meteorological data into energy variables, which were then used for the selection of events: extreme low European renewable energy production and extreme high European energy shortfall. Fig. 2 shows a flowchart indicating the way meteorological data and societal boundary conditions were combined to calculate daily wind and solar energy production, and energy demand.

In the model, the daily potential for renewable energy production (E_{pot}, no units) is computed first, for wind and solar sources separately (W_{pot} and PV_{pot}, respectively). The potential for wind and solar energy production solely depends on the meteorological conditions at day t. When the energy potential is multiplied by the spatial distribution of wind turbines and solar panels (the installed capacity, IC in TW), and total operational time (t_{oper} in hours day^{-1}) this results in an estimate of energy production (P in TWh day^{-1}):

$$P(t) = E_{pot}(t) \times IC \times t_{oper}(t), \tag{1}$$

as in Jerez et al. [16]. All calculations were done for each grid cell separately, indices x and y were excluded from all equations in this section for clarity. Wind and solar energy production were calculated separately, and then summed to provide an estimate for total energy production per grid cell per day. Total energy production was then integrated over the European domain under consideration, which resulted in the first impact variable time series from which events were selected. Further details for the calculation of wind energy production

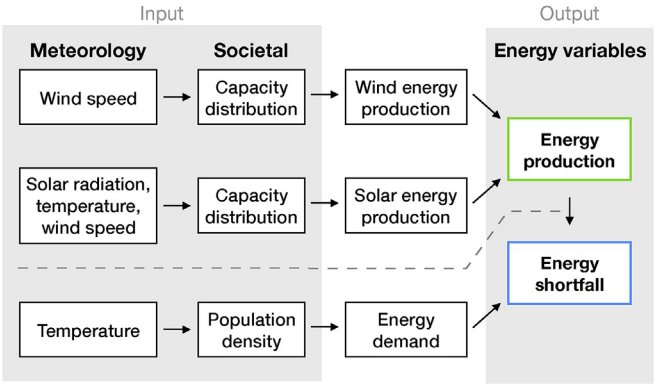

Fig. 2. Flowchart of the energy model design; more details are provided in the main text (Section 3). The model uses daily meteorological input data (first column) and societal boundary conditions (second column) to produce daily estimates of renewable energy production and energy demand (third column). These variables are then used to calculate two impact variables which are used for event selection (fourth column, Section 2).

and solar energy production are given in Sections 3.1 and 3.2.

Daily temperature-dependent energy demand was calculated using an empirical regression model, which was calibrated based on historical demand data from the European Network of Transmission System Operators for Electricity (ENTSO-E), European population density (GPWv4) [35], and temperature from the ERA-interim reanalysis product [32]. Model details are provided in Section 3.3.

Energy shortfall (S in TWh day^{-1}) or residual load, was defined to be the difference between energy demand (D in TWh day^{-1}) and total renewable energy production from wind and solar sources:

$$S(t) = D(t) - P(t). \tag{2}$$

Energy shortfall was used as the second impact variable time series from which events were selected for further study.

The analysis is based on a projected distribution of wind turbines and solar panels over a western European region. The region under consideration included 15 countries (Austria, Belgium, Denmark, France, Germany, Ireland, Italy, Luxembourg, the Netherlands, Norway, Portugal, Spain, Sweden, Switzerland and the United Kingdom, area not shaded grey in Fig. 3) and associated shallow offshore areas (sea floor depth up to 66 m). This projected spatial distribution of installed renewable energy capacity (IC in Eq. (1)) is based on the large scale renewable energy sources scenario from the e-Highway2050 project [19], which takes into consideration current installed capacity, future plans on a country-by-country level, and geographic land use data. The distribution as used here includes 378 GW onshore wind turbines, 101 GW offshore wind turbines (Fig. 3a), 120 GW rooftop solar panels and 42 GW utility-scale solar power plants (Fig. 3b). Total installed capacity in the domain is thus about 75% wind energy and 25% solar energy based. To quantify the sensitivity of our results to the spatial distribution of installed capacity (Section 6.2), a uniform placement of all capacity over land and offshore regions was also considered (SI Fig. S3).

3.1. Wind energy production

10 m wind speeds were scaled to wind speeds at wind turbine hub height by means of the power law profile:

$$V(h, t) = V(h_0, t)\left[\frac{h}{h_0}\right]^{\alpha}, \tag{3}$$

with h the hub height (m), h_0 the reference height (10 m) and α the roughness parameter. For onshore regions: $h = 80$ m and $\alpha = 0.143$; for offhore regions: $h = 120$ m and $\alpha = 0.11$ [16,36].

Given the wind speed at hub height ($V(h)$ in m s^{-1}), a power curve was used to determine the wind energy potential (W_{pot}, no units):

$$W_{pot}(t) = \begin{cases} 0 & \text{if} \quad V(t) < V_{ci}, \\ \frac{V(h,t)^3 - V_{ci}^3}{V_r^3 - V_{ci}^3} & \text{if} \quad V_{ci} \le V(t) < V_r, \\ 1 & \text{if} \quad V_r \le V(t) < V_{co}, \\ 0 & \text{if} \quad V_{co} \le V(t), \end{cases} \tag{4}$$

with V_{ci} the cut-in wind speed (taken to be 3.5 m s^{-1}), V_r the rated wind speed (13 m s^{-1}), and V_{co} the cut-out wind speed (25 m s^{-1}). To describe the shape of the non-linear part, a cubic power curve was followed [16,37], this assumes an ideal velocity power proportionality. The use of a cubic power curve has been shown to be a reasonable estimation for existing wind turbines [38]. Wind energy potential as a function of wind speed at hub height is shown in SI Fig. S1 Wind turbines can operate day and night, therefore $t_{oper} = 24$ hours day^{-1}, downtime for maintenance was not considered.

3.2. Solar energy production

Solar power potential (PV_{pot}, no units) was calculated following:

$$PV_{pot}(t) = P_R(t)\frac{G(t)}{G_{stc}}, \tag{5}$$

with P_R the performance ratio (no units), G the incoming solar radiation (W m^{-2}) and G_{stc} the incoming radiation under standard test conditions (1000 W m^{-2}) [14,16,39]. The performance ratio negatively depends on the temperature of the solar cell (T_{cell} in °C). In turn, cell temperature depends on the mean daytime air temperature ($T_{a,day}$ in °C), incoming solar radiation and wind speed:

$$P_R(t) = 1 + \gamma[T_{cell}(t) - T_{ref}], \tag{6}$$

in which

$$T_{cell}(t) = c_1 + c_2 T_{a,day}(t) + c_3 G(t) + c_4 V(t), \tag{7}$$

with constants $\gamma = -0.005$, $T_{ref} = 25$°C, $c_1 = 4.3$°C, $c_2 = 0.943$, $c_3 = 0.028$°C m^2 W^{-1} and $c_4 = -1.528$°C s m^{-1} [40]. Furthermore, $T_{a,day} = [T_{a,mean} + T_{a,max}]/2$ at 2 m height, G on a horizontal plane at the surface (neglecting potential tilt of solar panels) and V at 10 m height. The performance ratio as a function of daytime air temperature, wind speed and incoming radiation is shown in SI Fig. S2.

Solar panel operational time is determined by day length, dependent on the day of year and latitude. The CBM model as described in Ref. [41] was used to determine t_{oper} for the solar energy calculations, again downtime for maintenance was not considered. Daily-averaged values of incoming solar radiation (G) were corrected to only take into account hours of day where the sun is above the horizon.

3.3. Energy demand

A logistic smooth transition regression model [42] was used to describe the relationship between energy demand (D) and mean daily air temperature ($T_{a,mean}$) [43]. This model allows for a smooth transition between two linear regimes: electrical heating requirements due cold temperatures, and electrical cooling requirements due to warm temperatures:

$$D(t) = [\alpha_1 + \beta_1 T_{a,mean}(t)][1 - F(t)] + [\alpha_2 + \beta_2 T_{a,mean}(t)]F(t), \tag{8}$$

with α_1, α_2 the zero-crossing and β_1, β_2 the slope of these two linear regimes. The smoothing function (F) between the two linear regimes is given by:

$$F(t) = [1 + exp[-\zeta[T_{a,mean}(t) - c]]]^{-1}, \tag{9}$$

with ζ the smoothing factor and c the inflection point.

The model was calibrated based on historical ENTSO-E data (2006-

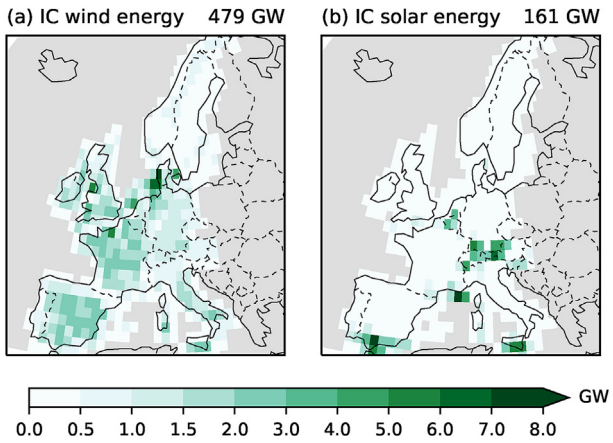

Fig. 3. Spatial distribution of installed capacity of (a) on- and offshore wind turbines, and (b) rooftop solar panels and utility-scale solar power plants (GW/grid cell) in the projected distribution. Note irregular colourbar, grey shading denotes land surface/ocean areas with zero installed capacity, value in the top right corner indicates total installed capacity.

2015[1]) aggregated over the 15 countries considered and a regional mean population-weighted 2 m air temperature from ERA-interim [32]. Population density as in the year 2015 [35]. Observed variations in energy demand depend on more than air temperature alone [17,25]. Therefore the days that systematically result in outliers were removed: all Saturdays and Sundays (no office work, less industry), the month August (summer holidays) and the Christmas and New Years' period (holidays, period taken to be 21 Dec - 6 Jan). Further outliers (e.g. due to national bank holidays) were discounted by using a robust linear regression fitting method. To remove the effects of the electrification of societies, the observed demand data were detrended prior to fitting. The following model parameters were determined for the European region under consideration: $\alpha_1 = 8.91$ TWh day^{-1}, $\beta_1 = -0.10$ TWh day^{-1} °C^{-1}, $\alpha_2 = 6.78$ TWh day^{-1}, $\beta_2 = 0.02$ TWh day^{-1} °C^{-1}, $\zeta = 0.52$°C^{-1}, $c = 11.17$°C. The model reproduces the historical variability of demand quite well (Fig. 4), the correlation coefficient of observed versus modelled demand is 0.88, the root mean square error is 0.29 TWh day^{-1}. Energy demand is lowest, 7.1 TWh day^{-1}, at 15.5 °C.

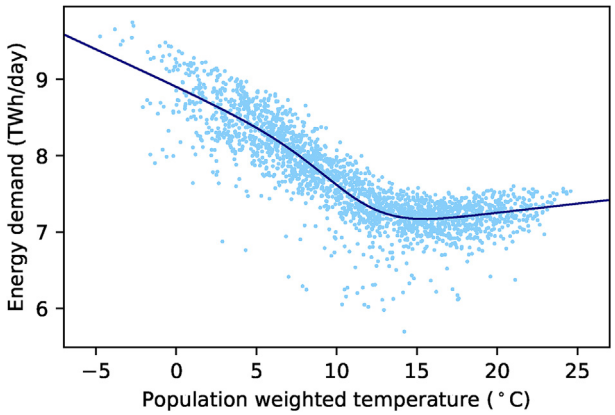

Fig. 4. Energy demand (TWh day^{-1}) as a function of regional-mean population weighted daily air temperature (°C). Light blue dots show the historical ENTSO-E data (systematic outliers removed as discussed in the text), dark blue line shows the fitted model.

4. Extreme low renewable energy production events

4.1. Annual cycle

Based on the EC-Earth present-day large ensemble experiment, 2000 years of daily wind energy production and solar energy production were calculated in the European domain under consideration. Annual mean daily wind energy production is 2.1 TWh day^{-1}, with higher values in winter than in summer (December-January-February, DJF, mean: 3.0 TWh day^{-1}, June-July-August, JJA, mean: 1.2 TWh day^{-1}, Fig. 5a). These values are slightly lower than what is found based on ERA-interim data (annual daily mean 2.6 TWh day^{-1}), the bias is approximately constant throughout the year. Solar energy production is on average 0.7 TWh day^{-1} for both EC-Earth and ERA-interim, with higher values during summer when days are longer and incoming radiation is higher (DJF mean: 0.3 TWh day^{-1}, JJA mean: 1.0 TWh day^{-1}, Fig. 5b). In the annual average, about 76% of the total production is from wind energy. This value is somewhat lower than what was expected given the wind-solar split in installed capacity, the discrepancy is mainly caused by a low wind speed bias over land areas.

For the development of a stable and secure power system with high penetration of variable renewable energy, it is the variability with respect to the seasonal mean that is of largest interest. Wind energy production exhibits greater variability than solar energy production (Fig. 5a,b), with standard deviations (st.devs.) of 1.2 TWh day^{-1} and 0.3 TWh day^{-1} respectively. As for mean wind energy production, variability of wind energy production peaks in the winter season (DJF st.dev.: 1.2, JJA st.dev.: 0.7 TWh day^{-1}). The full range of variability in winter is 0.2–7.9 TWh day^{-1}, the theoretical maximum for the assumed installed capacity is 11.5 TWh day^{-1}. Modelled variability is slightly lower than variability in the ERA-interim dataset (annual st.dev. 1.4 and 0.3 TWh day^{-1} for wind and solar respectively).

Variability of total energy production (Fig. 5c) is most like that of wind energy due to the relatively larger mean and higher variability from the wind compared to the solar source. Mean total energy production in winter exceeds that of the summer (means: 3.3 versus 2.2 TWh day^{-1}) and variability is largest in winter (st.devs.: 1.2 versus 0.7 TWh day^{-1}). Days with lowest total energy production occur in winter (Fig. 5c), in contrast to days with lowest wind energy production which occur in summer (Fig. 5a). Summertime solar energy production is responsible for this difference in seasonality (Fig. 5b). Tables including all reported mean and st.devs. in this section are included in the SI, to facilitate further comparison between modelled and ERA-interim data.

To select high-impact events a threshold for the 1-in-10 year 1-day low energy production event is determined (0.6 TWh day^{-1}, dashed line in Fig. 5c). All days below this threshold are selected (by design 200 out of 2000×365 days in total). The selected 1-day events fall in extended winters season (October to February), with 67% occurring in November or December.

4.2. Meteorological conditions

The mean meteorological conditions ('composites') are calculated for the 200 selected 1-in-10 year 1-day low energy production events, to determine which weather patterns cause the lowest energy production. During the selected low energy production events, a large-scale high pressure system is situated over central and eastern Europe (Fig. 6d). The exact location, shape and magnitude of this system varies between individual events. Due to the lack of pressure gradients, 10 m wind speeds are below normal over most of the region considered (negative anomalies in Fig. 6d), most notably over the North Sea area and west of the British Isles where a large portion of the offshore wind turbines is situated (Fig. 3a). Over land, where surface friction leads to lower wind speeds, the absolute wind speed is close to or below the cut-in wind speed of the turbines. The timing of 1-day low energy production events in the extended winter season, means solar energy production is low by default due to short day lengths (Fig. 5b). Lower than normal incoming solar radiation in the Mediterranean region decreases solar energy production further during the events (negative anomalies in Fig. 6h).

Given the relation between 10 m wind speed, incoming solar radiation and energy production (Eqs. (3)–(7)), it is obvious that these meteorological conditions indeed lead to low total energy production. Wind energy potential is lower than normal in the entire domain considered, over the North Sea it is 63% below normal. The solar energy potential in the Mediterranean region is lower than normal by 3%. This all leads to only 0.6 TWh day^{-1} of renewable energy production in the entire European domain considered (Fig. 7a and 2.5 TWh day^{-1} lower than normal).

To verify the above results from the EC-Earth model, similar composite mean maps for four 1-in-10 year 1-day low energy production events in the ERA-interim dataset were computed. The meteorological state of the ERA-interim events (SI Fig. S4) is comparable to that found for the EC-Earth events (Fig. 6d,h): a high pressure system is situated over eastern Europe, lower than normal 10 m wind speeds in the North Sea area and southwest of the British Isles, and lower than normal solar radiation in southern Spain and France. Composite anomaly values are

[1] European energy demand data provided by ENTSO-E, downloaded from www.entsoe.eu/data/data-portal/, accessed 05-02-2018.

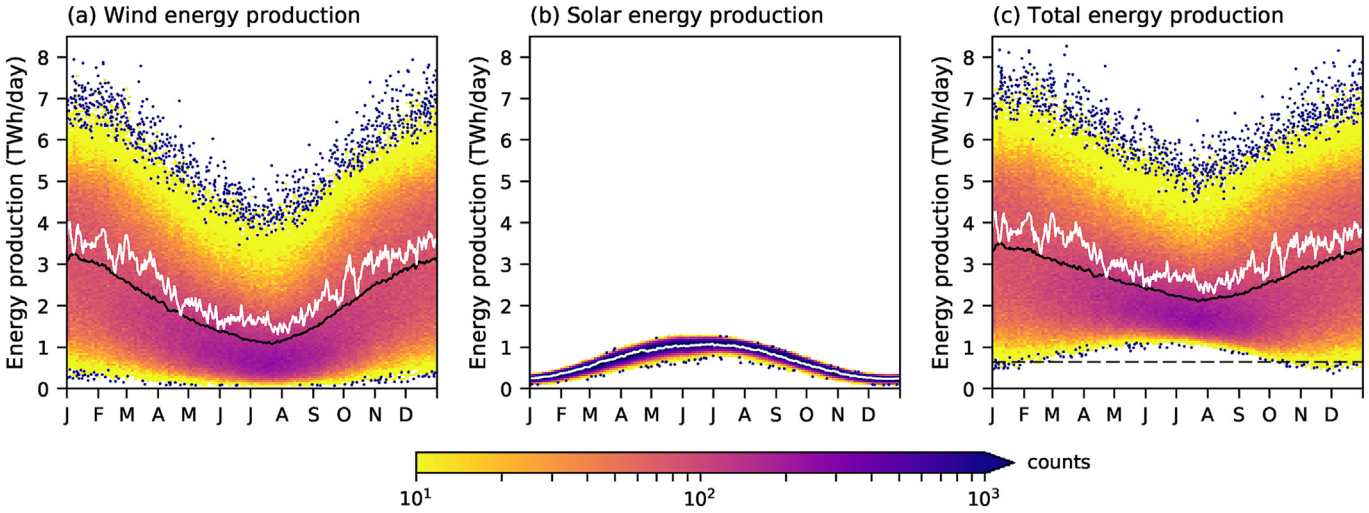

Fig. 5. 2D histogram of (a) daily wind energy production, (b) daily solar energy production, (c) daily total energy production (TWh day^{-1}). Colours show the counts in each bin (bin width is 3 days, bin height is 0.05 TWh day^{-1}), blue dots shows outliers (1 event per bin), the continuous black line shows the mean annual cycle, the white line shows the mean annual cycle from ERA-interim data (1979–2017). The threshold for 1-in-10 year high-impact events based on extreme low total energy production is indicated with a horizontal dashed line in (c).

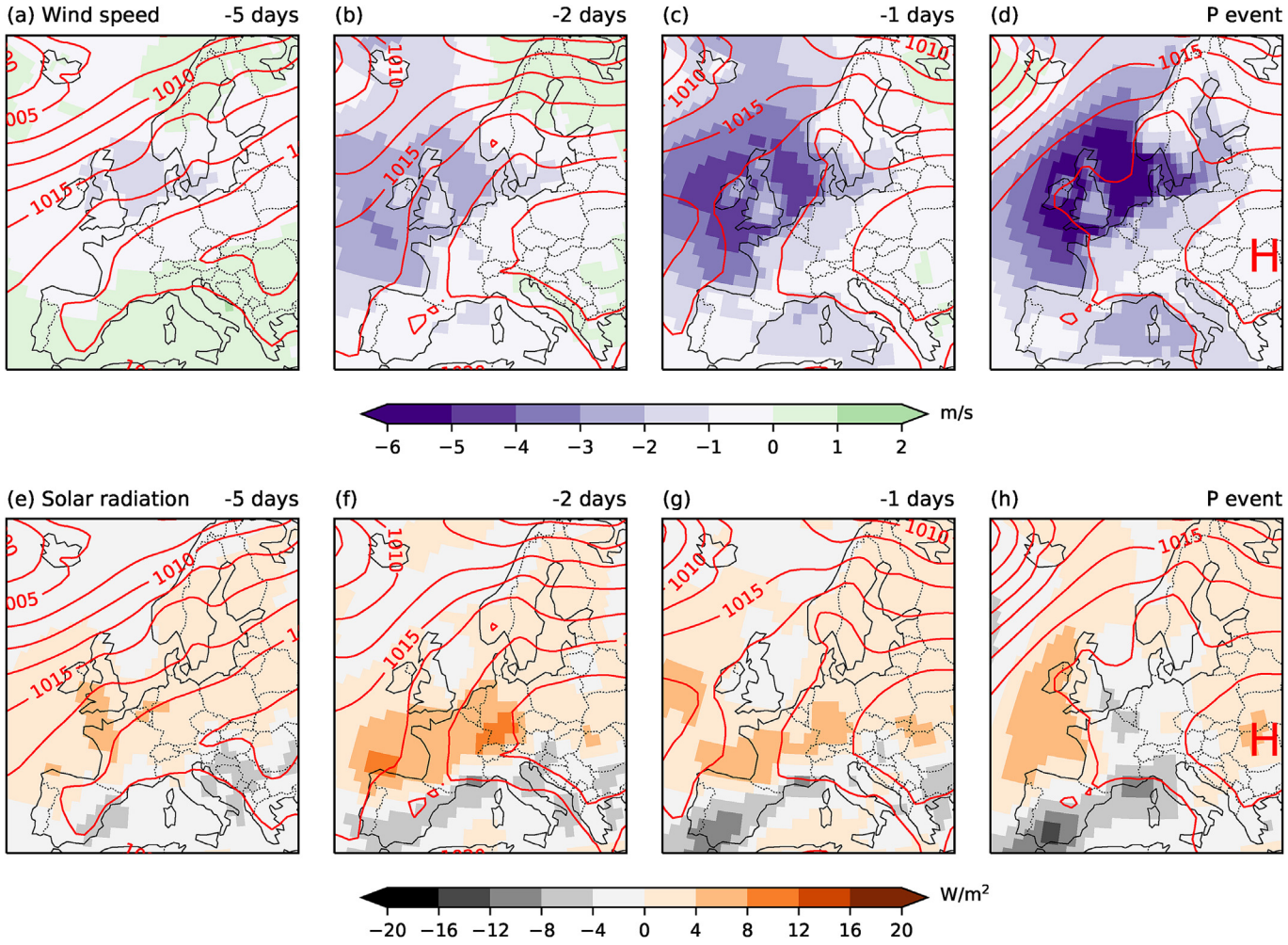

Fig. 6. Composite mean maps of meteorological variables for low energy production events ('P events') with an average return period of 1-in-10 years. Colours show (a–d) anomalies of 10 m wind speed (m s^{-1}), and (e–h) anomalies of incoming solar radiation (W m^{-2}), red contours are isobars of sea level pressure (contour interval 2.5 hPa). Time lags shown are (a,e) event − 5days, (b,f) event − 2 days, (c,g) event − 1days, and (d,h) selected low energy production event.

larger in ERA-interim than in EC-Earth, this may be related to the fact that the composite is an average over four rather than 200 events. Averaging over four events, as done for the ERA-interim data, provides limited information on the full distribution of high-impact events. In the SI it is shown that these four ERA-interim events fall within the distribution of modelled events from EC-Earth in terms of both surface pressure pattern and North Sea 10 m wind speed anomalies (SI Fig. S6).

4.3. Temporal development

Although the high-impact events are selected on the basis of extreme low 1-day renewable energy production, the high pressure system driving the low production is longer lived (Fig. 6a–d). From about 6 days preceding the events the high pressure starts to build, peaking around the event and disappearing 3 days after. 10 m winds slacken in the North Sea area about 3 days before the event, and further weaken over a larger area in the following days (Fig. 6b–d). 10 m wind speeds return to normal strength about 3 days after the event. These meteorological developments cause a sharp decline in energy production in the days surrounding the event day (Fig. 7a). Two days before the selected event days, composite mean total energy production is 2.0 TWh day^{-1} (1.1 TWh day^{-1} lower than normal), though there is large variability between individual events (0.5–5.0 TWh day^{-1}). Two days after the event total energy production is 2.2 TWh day^{-1} (0.9 TWh day^{-1} lower than normal).

Some of the selected high-impact low production events are indeed 1-day extreme events, e.g. the 3-day production time series: 2.8-0.6-2.6 TWh day^{-1} (orange line in Fig. 7a). However, there are cases in which low energy production immediately precedes and proceeds the selected events. For the 200 selected low production events, there are two cases in which three individual 1-in-10 year 1-day events are clustered, e.g. the 3-day production time series: 0.5-0.5-0.6 TWh day^{-1} (red line in Fig. 7a). There are seventeen cases of two consecutive 1-day events (including the 3-day events mentioned above).

The potential societal impact of low energy production and the design of future power systems greatly depends on the duration of these events. To investigate events of longer duration, the same impact-based selection procedure as before is applied to select events of 7-days low energy production (7-days mean production threshold: 1.2 TWh day^{-1}, Fig. 7b) and 14-days low energy production (14-days mean production threshold: 1.4 TWh day^{-1}, Fig. 7c). The 7-days and 14-days events are dynamically comparable to the 1-day events: a large high pressure system over central Europe, associated with lower than normal 10 m wind speeds in the North Sea area and reduced incoming radiation in southern Europe (not shown). These periods of prolonged high pressure are referred to as 'atmospheric blocking'. Such blocks cause long periods of similar meteorological conditions, e.g. many days of low wind speed, this leads to a general increase in the risk of the occurrence of extreme events [44], which is also the case here. Longer events tend to occur earlier in the season. The occurrence of 1-day events peaks in November, that of 7-days events in October and that of 14-days events in September (Fig. 7d).

5. Extreme high energy shortfall events

5.1. Annual cycle

The second energy impact variable that is considered is energy shortfall. Before discussing energy shortfall, first the annual cycle of energy demand and the share of renewable energy in total demand in the 2000 year present-day large ensemble experiment is discussed. EC-Earth modelled daily energy demand peaks early in February due to cold temperatures (DJF mean: 8.5 TWh day^{-1}, st.dev.: 0.2 TWh day^{-1}, Fig. 8b), and is lowest mid-summer (JJA mean: 7.2 TWh day^{-1}, st.dev.: 0.1 TWh day^{-1}). The hard minimum boundary of energy demand in the summer months at 7.1 TWh day^{-1} is caused by the minimum in the energy demand model at 15.5 °C (Fig. 4). Any temperature change from that point, both higher and lower values, leads to an increase of energy demand.

The mid-summer minimum is not found in ERA-interim, which has two minima in the beginning of June and in late September. In ERA-interim, there is a slight rise in energy demand mid-summer due to electric cooling requirements. EC-Earth has a regional summer cold bias of 1.1 °C (JJA mean, population weighted regional mean) and therefore misses this summertime increase of demand. The demand maximum in winter is similar in EC-Earth and ERA-interim.

In the current model setup, energy demand (Fig. 8b) is higher than

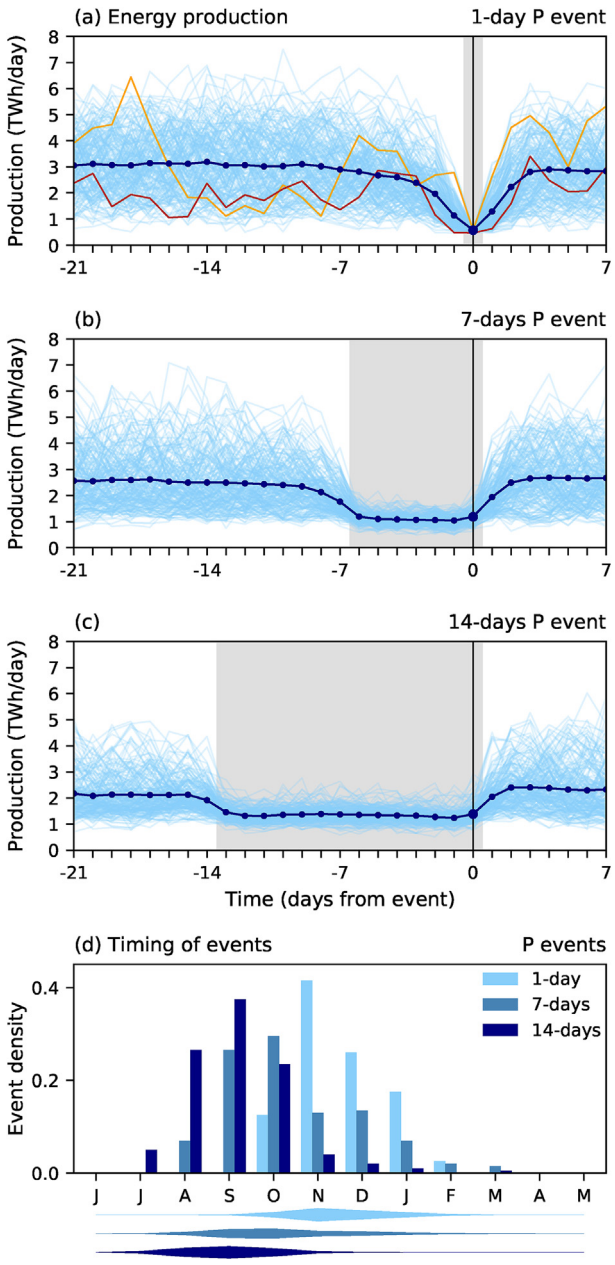

Fig. 7. (a–c) Time series of total energy production for (a) 1-day, (b) 7-days and (c) 14-days low energy production events with an average return period of 1-in-10 years. Light blue lines show time series around individual events, the dark blue line is the composite mean over all events, grey shading shows the duration of the event considered. Orange and red lines in (a) show specific individual events, see main text for details (Section 4.3). (d) Histogram indicating the timing of 1-, 7- and 14-days low energy production events, horizontal bars at the bottom show a kernal density estimate of these distributions.

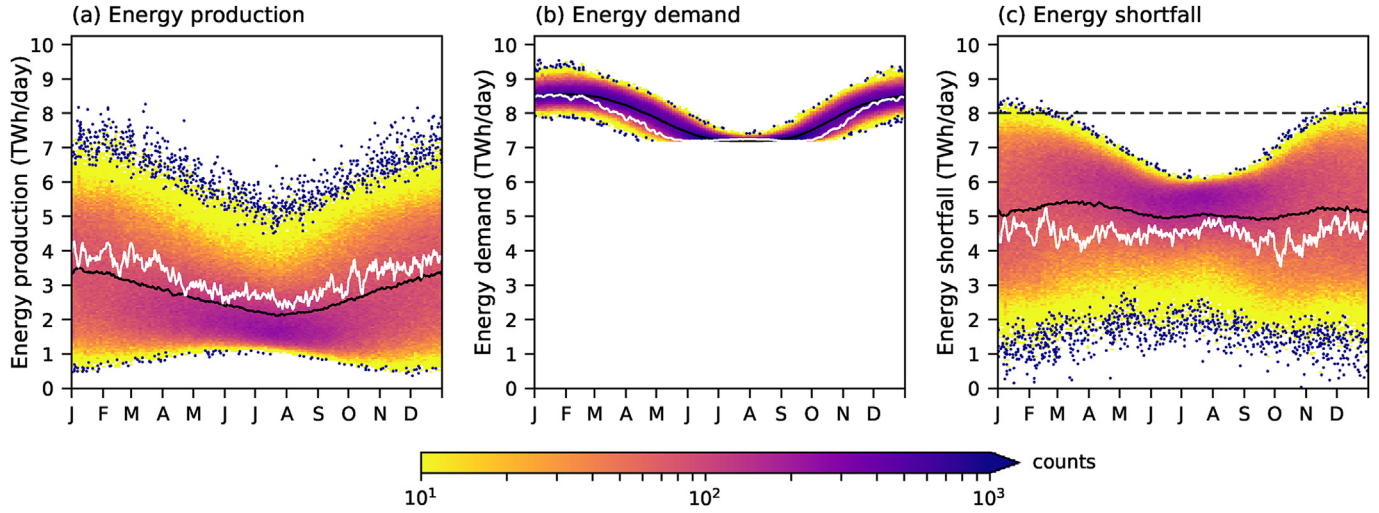

Fig. 8. As Fig. 5 but here for (a) daily energy production, (b) daily energy demand, (c) daily energy shortfall (TWh day^{-1}). The threshold in (c) here indicates the threshold for extreme high energy shortfall events.

energy production (Fig. 8a). The assumed projected distribution of installed capacity (Fig. 3) leads to an annual average share of renewable energy of 35% (day-to-day range from 4 to 100%) in EC-Earth. This is slightly lower than what results from ERA-interim data (average share of 42%), due to the lower modelled wind energy production (Section 4.1). We investigate the part of energy demand not met by renewable energy production, energy shortfall (Fig. 8c), further.

Ensemble mean 1-day energy shortfall is fairly constant throughout the year (5.1 TWh day^{-1}), though there is large variability around this mean (st.dev. 1.1 TWh day^{-1}, Fig. 8c). Due to higher variability in winter (DJF st.dev.: 1.3 TWh day^{-1}, JJA st.dev.: 0.7 TWh day^{-1}), all selected 1-day energy shortfall events occur from November to March, with 81% in December-January (event selection threshold: 8.0 TWh day^{-1}). The effect of including temperature-dependent demand in the event selection, is thus a shift of events to the coldest period of the year. Low energy production events occur mostly in November-December (Section 4.1).

5.2. Meteorological conditions

Similar to low energy production events (Section 4.2), the 1-day high energy shortfall events are characterised by a large-scale high pressure system (Fig. 9d), associated 10 m wind speed anomalies are comparable in magnitude and location (Figs. 9d and 6d). Incoming solar radiation is lower than normal in southern Europe, though above normal further north (Fig. 9h). These positive radiation anomalies were not found for the low energy production events (Fig. 6h). Mean energy production for the high shortfall events is 0.8 TWh day^{-1}, which is 0.2 TWh day^{-1} (36%) higher than energy production for the low energy production events. From an energy production perspective, the 1-in-10 year high energy shortfall events are 1-in-2.2 year events (899 occurrences in the 2000 year data set).

The 2 m temperature anomaly (Fig. 9l) is what sets the high energy shortfall events apart. The entire region considered is colder than normal, in places anomalies exceed −6 °C. Electric heating requirements for such cold episodes boost energy demand (Eqs. (8) and (9)). Mean energy demand for the high energy shortfall events is 8.9 TWh day^{-1}. This is not an exceptionally high value for energy demand, it has an average return period of 0.3 years (7763 occurrences), but combined with the simultaneous low energy production the higher demand leads to extreme energy shortfall. There is no significant temperature anomaly for the selected low energy production events (not shown). Mean energy demand for the low energy production events is therefore 0.5 TWh day^{-1} lower than for the high energy shortfall events.

Again the model results are verified with ERA-interim data. ERA-interim high shortfall events are characterised by a high pressure system (SI Fig. S5), though in contrast to EC-Earth the core lies over Ireland. The pattern of negative 10 m wind anomalies and incoming radiation anomalies are similar. The cold anomalies are substantially larger in the ERA-interim composite (exceeding 10 °C in central Europe), however the four ERA-interim events all fall within the full distribution of modelled events (SI Fig.S7).

5.3. Temporal development

The high pressure system leading to 1-day high energy shortfall events (Fig. 9a–d) develops slightly slower than that leading to 1-day low energy production events (Fig. 6a–d, Section 4.3). The associated 10 m wind anomalies (Fig. 9a–d) and incoming radiation anomalies (Fig. 9e–h) therefore appear a few days earlier. The reason is that it takes time to cool central Europe. With high pressures settling over Europe, the winds immediately die down. Temperatures drop slowly in response to a weak north-easterly flow bringing colder air and strong radiative cooling during clear skies at night dominating the above normal daytime solar heating.

This slow thermal response has consequences for the temporal development of energy shortfall. For 1-day shortfall events, energy production drops below normal values slightly earlier than production during low energy production events. Energy demand steadily increases over time in response to the falling temperatures (Fig. 9i-l), as expected this is not found for the low energy production events. The simultaneous reduction in energy production and growth of energy demand leads to an increase of energy shortfall around the event date (Fig. 10a). Low energy production events also display an increase in energy shortfall, though forced by decreasing energy production alone.

The 7- and 14-days shortfall events (Fig. 10b,c) are dynamically comparable to the 1-day events. They are forced by a large-scale high pressure system over central Europe, negative 10 m wind anomalies in the North Sea area, negative incoming radiation anomalies in southern Europe and colder than normal surface temperatures (not shown). In contrast to the low energy production events which undergo a shift in seasonality, the shortfall events occur at the same time of year independent of their length (Fig. 10d).

5.4. Co-occurring low production and high shortfall events

Given the relationship between energy shortfall and energy production (Eq. (2)), and the comparable meteorological situation for low

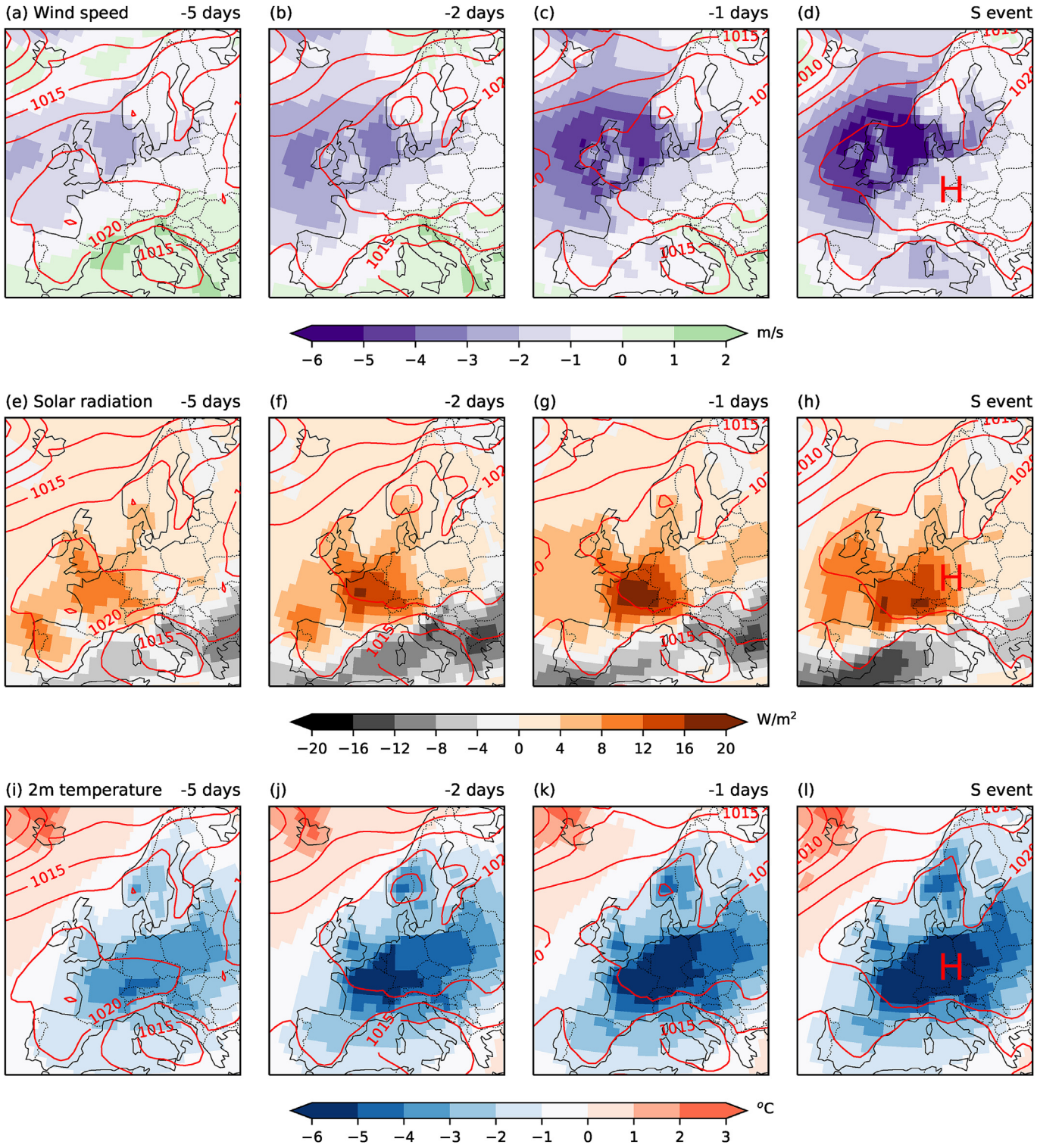

Fig. 9. As Fig. 6, but here for composite mean maps of meteorological variables for high energy shortfall events ('S events'). Colours here show (a–d) anomalies of 10 m wind speed (m s^{-1}), (e–h) anomalies of incoming solar radiation (W m^{-2}), and (i–l) anomalies of 2 m air temperature (°C).

energy production events and high energy shortfall events (Figs. 6 and 9, Sections 4.2 and 5.2), one may expect some co-occurrence of these high-impact events. However, there is no statistical relationship between energy production and energy demand (Fig. 11a), and there are no co-occurring extreme low energy production and extreme high energy demand events at 1-, 7- or 14-days time scales. The co-occurrence of extreme low energy production and extreme high energy shortfall is therefore investigated separately.

From Fig. 11b and c it is obvious that there is a relationship between energy production and energy shortfall. Correlations are stronger if the data is separated by season (1-day event correlation coefficients annual: $r = -0.87$, DJF: $r = -0.99$, JJA: $r = -0.99$), however because of the differences in timing of low energy production events and high energy shortfall events (Fig. 10d), the full year of data must be considered. The statistical relationship between low production and high shortfall is stronger for events of shorter duration than for events of longer

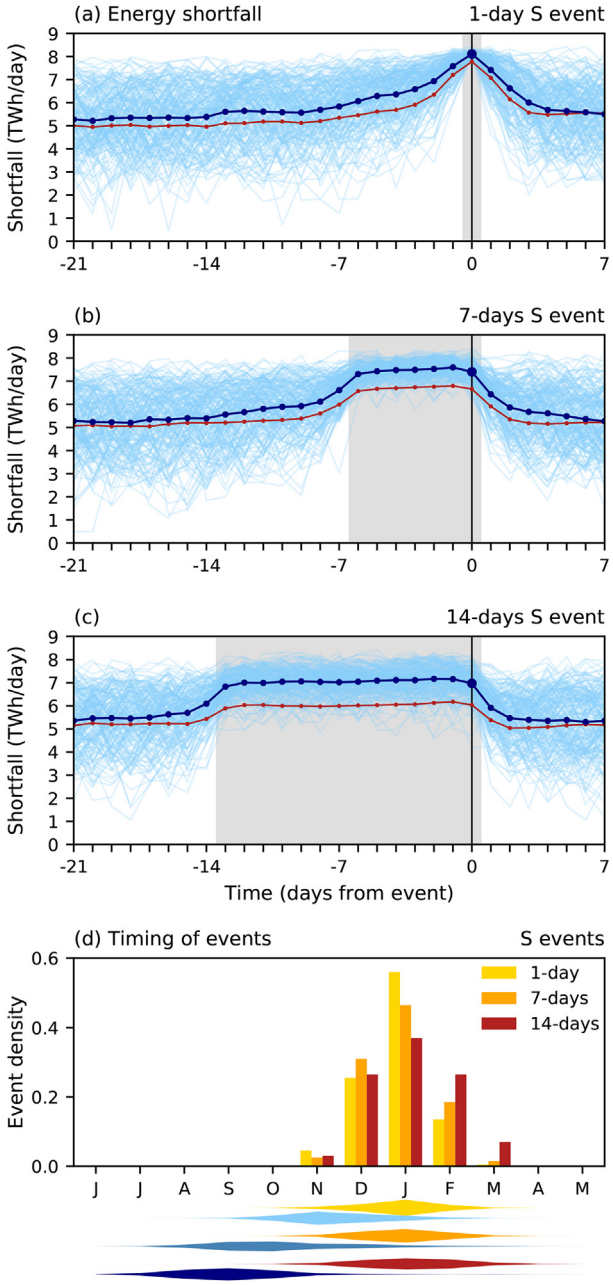

Fig. 10. (a–c) As Fig. 7a–c but here for time series of energy shortfall for high energy shortfall events. The dark red line shows the composite mean over the low energy production events. (d) As Fig. 7d but here for high energy shortfall events, colours have changed. Horizontal bars at the bottom show a Kernal density estimate of these distributions, in blue the distributions of low energy production events (as in Fig. 7d).

duration ($r = -0.87$, $r = -0.74$ and $r = -0.63$ for 1-, 7- and 14-days time scales respectively). Also, co-occurrence of extreme low energy production and extreme high energy shortfall events decreases for events of longer duration: 42 of 200 1-day events co-occur (21%, Fig. 11b), 39 7-days events (20%) and six 14-days events (3%, Fig. 11c). The cause for the decreasing strength of the linear relationship and decreasing co-occurrence is the shift of the season with highest chance of low energy production events for longer events that is not found for longer-lasting high shortfall events (Fig. 10d).

6. Sensitivity of results

6.1. Choice of global climate model

Global climate models are imperfect, this results in biases in simulated variables and simulated weather patterns. The results in Sections 4 and 5 are based on simulations with the EC-Earth global climate model [29]. These model results have been compared with similar analyses based on ERA-interim data, which provides some confidence in the robustness and relevance of the results (see SI). Further evidence for the robustness of results is provided by a repetition of the analysis with a different global climate model. All analyses presented in Sections 4 and 5 were repeated using the HadGEM2-ES [33] large ensemble under present-day conditions (see Section 2 and Fig. 1).

HadGEM2-ES has a larger bias of wind energy production than EC-Earth (annual mean HadGEM2-ES: 1.3 TWh day^{-1}, EC-Earth: 2.1 TWh day^{-1}, ERA-interim: 2.6 TWh day^{-1}) and performs similar in terms of simulating solar energy production (annual mean for all three: 0.7 TWh day^{-1}). The annual cycle of total energy production in HadGEM2-ES is largely comparable, though it peaks in February rather than January (EC-Earth and ERA-interim). Variability around the seasonal mean is closer to ERA-interim in the EC-Earth data (annual st.dev. HadGEM2-ES: 0.8 TWh day^{-1}, EC-Earth: 1.1 TWh day^{-1}, ERA-interim: 1.3 TWh day^{-1}). Despite these differences, the composite mean meteorological conditions and timing of selected low energy production events are remarkably similar to those from EC-Earth (Fig. 12a,b and 6d,h). There is a large high pressure system of approximately the same strength and in approximately the same location. In HadGEM2-ES the negative 10 m wind speed anomalies are slightly weaker over the North Sea area, incoming solar radiation anomalies are stronger than in EC-Earth. Low production events occur from October to February, with 76% in November-December (event selection threshold 0.5 TWh day^{-1}, compared to 0.6 TWh day^{-1} in EC-Earth). The temporal development of the high pressure system, associated surface anomalies and total energy production are comparable as well (Fig. 12c), though the decrease of energy production is larger in EC-Earth due to its larger mean production and higher variability.

HadGEM2-ES reproduces the ERA-interim annual cycle of energy demand (HadGEM2-ES DJF mean: 8.5 TWh day^{-1}, JJA mean: 7.3 TWh day^{-1}; ERA-interim DJF mean: 8.5 TWh day^{-1}, JJA mean: 7.2 TWh day^{-1}). The low energy production bias therefore leads to a high bias in energy shortfall. As was found for EC-Earth, ensemble mean energy shortfall is relatively constant throughout the year (5.8 TWh day^{-1}), the 1-in-10 year high shortfall event selection threshold is 8.4 TWh day^{-1} (8.0 TWh day^{-1} in EC-Earth). The composite mean high pressure system leading to high energy shortfall is similar to that found for EC-Earth (Figs. 12d,e and 9d,l), the associated cold temperature anomalies are larger in HadGEM2-ES than in EC-Earth. The distributions of pressure patterns, 10 m wind speed and temperature anomalies for all selected events in HadGEM2-ES and EC-Earth are included in the SI (SI Figs. S6,S7).

In HadGEM2-ES the co-occurrence of low energy production events and high energy shortfall events is less dependent on the length of the events (7, 6 and 5% of events for 1-, 7- and 14-days events respectively) as was found in EC-Earth data (Section 5.4). In HadGEM2-ES the shift to late summer/autumn for longer lasting low energy production events is smaller than that in EC-Earth. Consequently, there is more overlap in the timing of low energy production and high energy shortfall events of all lengths.

6.2. Spatial distribution of wind turbines and solar panels

The results in Sections 4 and 5 depend on the selection of events based on calculated values for energy production and energy shortfall. Energy production depends on the spatial distribution of wind turbines and solar panels (IC in Eq. (1)). The main results are not impacted if a

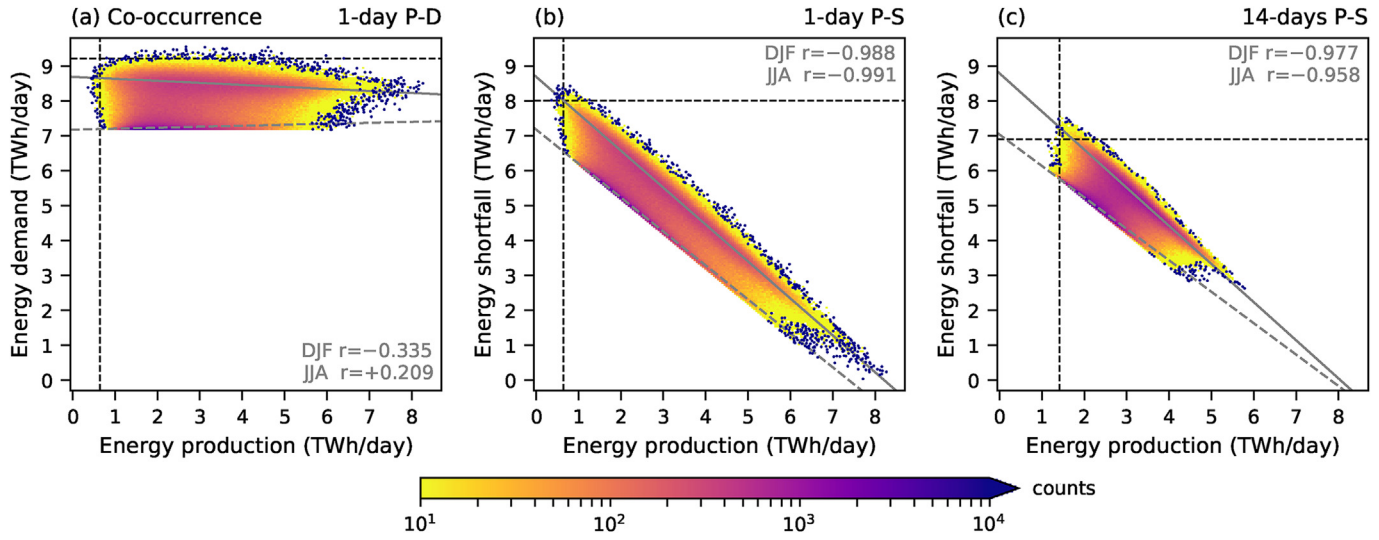

Fig. 11. 2D histogram comparing (a) energy production (TWh day^{-1}) and energy demand (TWh day^{-1}), and (b,c) energy production and energy shortfall (TWh day^{-1}) for (a,b) 1-day events and (c) 14-days events. Colours show the counts in each bin (bin width and height 0.05 TWh day^{-1}), blue dots show the outliers (1 event per bin), the solid grey line shows a fitted linear regression for DJF, the dashed grey line shows a fitted linear regression for JJA (correlation coefficients are noted), dashed black lines show the 1-in-10 year event thresholds for both distributions (taking into account minimum event separation in (c)).

different spatial distribution of installed capacity had been used for the study, showing the robustness of the presented results. Here the events selected based on the projected distribution (Fig. 3) are compared to events selected based on the uniform distribution of wind turbines and solar panels (SI Fig. S3, described in Section 3).

Mean renewable energy production based on the projected distribution is 2.7 TWh day^{-1} (full range: 0.4 to 8.3 TWh day^{-1}, Fig. 5c) and 2.8 TWh day^{-1} based on the uniform distribution (full range: 0.4 to 7.3 TWh day^{-1}, Fig. 13a). The projected distribution has a longer tail with high production, but its mean production is lower. On average, the uniform distribution thus more evenly harvests the available wind and solar resource and better compensates below average yields in some places with higher yields in other places.

The selected low energy production events of interest here are not sensitive to the spatial distribution of installed capacity. If event selection is repeated based on extreme low energy production from the uniform distribution, 69 of 200 1-day events have the same date (Fig. 13b), a further 14 events are within a week from each other. The meteorological conditions described in Section 4 are comparable when high-impact events based on the uniform distribution are investigated.

Energy shortfall is defined as the difference between energy demand and energy production (Eq. (2)). Since modelled demand is only temperature dependent, it is not sensitive to the distribution of installed capacity. Therefore, the sensitivity of energy shortfall to the distribution of installed capacity is comparable to the sensitivity of energy production. Mean shortfall is 5.1 TWh day^{-1} for both distributions (Fig. 13c). If event selection is repeated for shortfall, 81 of 200 1-day events have the same date between the two distributions, an additional 17 events occur within a week of each other. The reported meteorological conditions in Section 5 are not impacted.

6.3. Influence of climate change

Next the influence of further global climate change on European renewable energy production and energy demand is investigated. To do so, two large ensemble experiments, each 2000 years, both generated with the EC-Earth global climate model are compared. The two ensembles differ in their GMST, one representing the present-day climate (analysed in Sections 4 and 5) and one a projected pre-industrial + 2 °C warming future climate, see Section 2 for details.

Both wind energy production and solar energy production do not show much change (mean wind energy production of 2.1 becomes 2.0 TWh day^{-1}, mean solar energy production remains 0.7 TWh day^{-1}), and also variability does not change (st.devs. unchanged). The small shift of the mean is outweighed by much larger variability, indicating that renewable energy production in a future warmer climate is comparable to that in the present-day climate. Previous studies on wind energy production give projections of varying sign, though all note changes are small taking into account model biases and strong interannual variability [18,45–49]. Solar energy projections note mean increases in southern Europe [50,51], though the direction of change is dependent on atmospheric circulation [18].

Energy demand, calculated using the model as in Section 3.3, is projected to decrease in the winter season (DJF mean demand of 8.5 becomes 8.4 TWh day^{-1}). Rising temperatures lead to a decrease in electrical heating requirements. As a result, wintertime energy shortfall as defined in this paper will decrease. The temperature-related trend in energy demand from this simple model is in agreement with reported trends from more complex energy demand models [24,52,53]. Summertime energy demand does not change in these simulations (7.2 TWh day^{-1} in both ensembles), the demand model used here is not very sensitive at high temperatures (i.e. weak slope for temperatures above 15.5 °C in Fig. 4).

Finally, the occurrence of extreme events as discussed in Sections 4 and 5 under climate change is investigated. To do so, Generalized Extreme Value (GEV) distributions are fitted to 2000 annual extreme events (block minima/maxima) [54]. As expected, given the above result that wind and solar energy production do not show large changes in response to further global climate change, there is no change in the occurrence of extreme low energy production events (Fig. 14a). Changes are found in the risk of occurrence of extreme energy shortfall events, in line with decreased wintertime energy demand (Fig. 14b). Given the energy model used here, the risk of extreme energy shortfall decreases. The 1-in-10 year energy shortfall event at 8.0 TWh day^{-1} in the present-day climate becomes a 1-in-17 year event in a 2 °C warmer climate. These results are consistent with projections that show no change or slight decreases in winter atmospheric blocking under climate change [44] and increasing winter temperatures [55].

It is important to realise that the energy demand model used here assumes a historical (2006–2015) relationship between temperature variations and electrical consumption that will very likely change due to future changes in electrical consumption and power system design. It

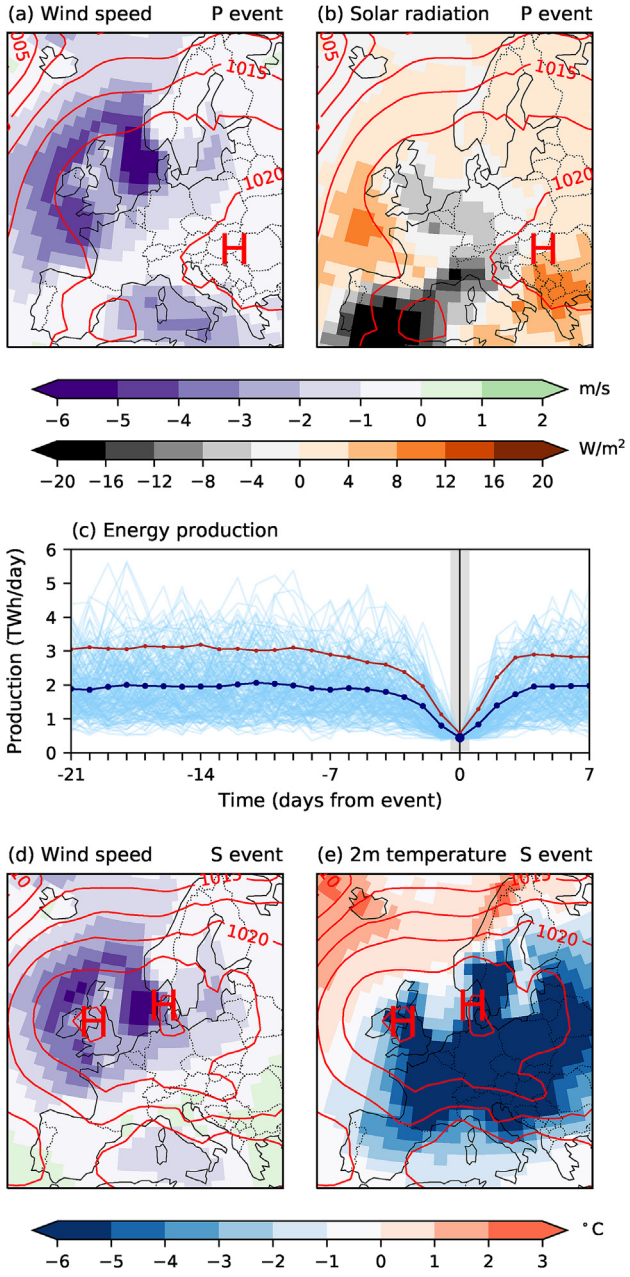

Fig. 12. Reproduction of selected panels of Figs. 6, 7 and 9, but here based on data from the HadGEM2-ES present-day large ensemble experiment. (a,b,d,e) Composite mean maps of meteorological variables for (a,b) low energy production events (as in Fig. 6d,h), and (d,e) high energy shortfall events (as in Fig. 9d,l). (a,d) show anomalies of 10 m wind speed (m s^{-1}), (b) shows anomalies of incoming radiation (W m^{-2}), (e) shows anomalies of 2 m air temperature (°C). (c) Time series of energy production for low energy production events (TWh day^{-1}), light blue lines show individual events for HadGEM2-ES, dark blue line the HadGEM2-ES composite mean, red line shows the composite mean for EC-Earth (as in Fig. 7a).

is therefore recommended that climate change induced changes in energy demand and energy shortfall are revisited in future studies (see also Section 7). In the current setup, there is room for increased electrical consumption during summer months, because summertime maximum energy shortfall is 2 TWh day^{-1} lower than its winter peak (Fig. 8c).

7. Discussion

The analysis in this paper may be improved upon by using a climate model of higher horizontal, vertical and temporal resolution. This would allow more detailed analysis of spatial variability [56], more accurate analysis of wind speeds at turbine height [36,57], and allow the analysis of sub-daily variability. A comparison with higher resolution climate model data can provide insights into the importance of these different resolutions. In general, large-scale atmospheric circulation patterns are captured relatively well in coarse global climate models, there is thus confidence in the risk that these high pressure systems pose for European energy security. Comparable event analysis for high shortfall events in Great Britain based on reanalysis data identified similar weather systems leading to high risk there [25]. There is evidence that high resolution models better capture large scale processes related to atmospheric blockings [44,58]. The use of daily-averaged data from the climate model leads to an underestimation of the variability of wind energy production. A sensitivity analysis shows that the selection of extreme low energy production events is not impacted. Below the cut-in wind speed of wind turbines, small changes in the wind speed do not lead to changes in wind energy production.

Biases in modelled meteorological variables negatively impact the quality of modelled energy variables. Modelled 10 m wind speeds in EC-Earth are lower than those in ERA-interim. These biases amplify in the calculation of energy potential, because winds speeds frequently fall in the non-linear energy production regime of wind turbines (Eq. (4)). A low bias in wind energy production, combined with a slight overestimation of solar energy production due to cooler summer temperatures, leads to a skewed ratio of wind-to-solar production (wind is 76% of total here, expected to be around 85–90% given the assumed power mix). A sensitivity analysis shows that the threshold level for extreme low energy production is somewhat influenced by this bias, and that the seasonal cycle of the lower boundary of the histogram of energy production (Fig. 5c and 0.5 TWh day^{-1} in DJF, 1.1 TWh day^{-1} in JJA) is exaggerated due to this bias. However, the season of extreme event occurrence remains the extended winter, therefore event selection and the presented results are not impacted.

In the energy model a projected distribution of wind turbines and solar panels was assumed, in this distribution the ratio of installed capacity is 75% wind- and 25% solar-based. Changes to the mix of wind versus solar energy influence the annual cycle of total energy production and the season in which extreme low production events occur (Fig. 5a–c can be interpreted as showing a 100% wind-based system, a 100% solar-based system, and a mixed system at 75 %–25% installed capacity). Assuming the spatial distribution as in the present energy model, the influence of the strong annual cycle of solar radiation determines the timing of events for all power mixes with more than 10% solar capacity. For power systems with other weather-dependent sources of energy, e.g. wave power generation, the analysis method developed here can be applied to identify the situations that lead to high societal risk then.

It was assumed that the height of wind turbines is 80 m over land and 120 m in offshore regions, but likely wind turbines will be higher in the future. Higher turbines can harvest higher wind speeds (Eq. (3)) leading to higher absolute energy production (Eq. (4)) and lower values of energy shortfall (Eq. (2)). However, relative difference between regions are not affected, therefore the selection of events and the meteorological conditions described are not impacted by assumed turbine height.

The energy demand model (Section 3.3) was calibrated using historical demand data for the years 2006–2015. A further electrification of society has not been taken into account. Besides a steady increase of weather-independent energy demand, increases in the weather-dependent-part of energy demand are also foreseen [24,59]. In the design of the future power system, it is important to take into account projected (weather-dependent) energy demand. Further work may investigate

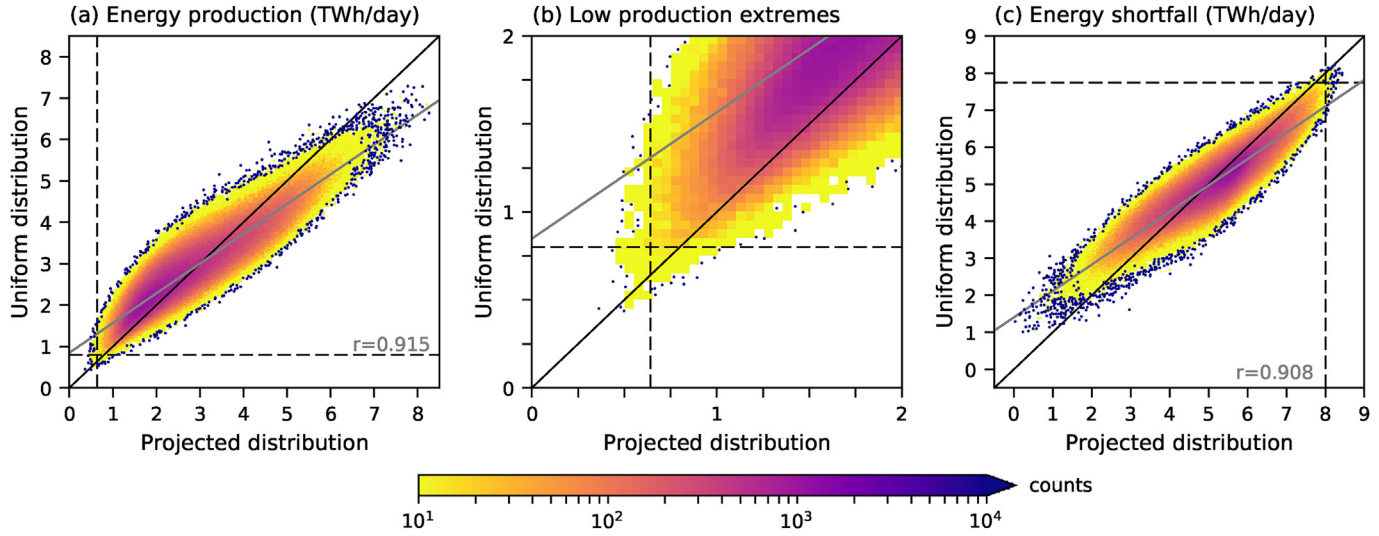

Fig. 13. 2D histogram comparing (a,b) 1-day energy production (TWh day^{-1}) and (c) 1-day energy shortfall (TWh day^{-1}) for two different distributions of installed capacity: the projected distribution (Fig. 3) and a uniform distribution (SI Fig. S3). Colours show the counts in each bin (bin width and height is 0.05 TWh day^{-1}), blue dots show the outliers (1 event per bin), the continuous black line shows the diagonal, the grey line shows a fitted linear regression (correlation coefficient noted), dashed lines show the 1-in-10 year event thresholds for both distributions.

how the high shortfall events described here will change if future scenarios for weather-dependent energy demand are taken into account. If the dependence of energy demand on temperature increases, i.e. β_1 becomes more negative (Section 3.3, Eq. (8)), temperature anomalies would have relatively larger effects on shortfall than quantified in Section 5. Furthermore, the energy model in its current form does not take into account limitations in the transport of energy between regions (copper-plate assumption), future work may investigate co-variability of regions and vital connections between energy producing regions.

An analysis of the meteorological conditions leading to high risk for future European energy security has been presented. The extreme impacts-based approach used here is fundamentally different from previous meteorology-centred approaches and from seasonal or annual average analyses [11,12,14,15,17,18,25,28,45,47,48,60–62]. Though mean conditions and projected changes therein are relevant to determine the feasibility of renewable energy as the main source of energy in the future, ultimately it is the variability around the mean and extreme events as described here that determine the flexibility requirements of a highly-renewable power system and should be governing in the design of these systems. The noted level of extreme energy shortfall events at different time scales may contribute to future studies regarding back-up energy storage and back-up installed capacity requirements. The importance of long time series or large ensemble data sets for assessing the impacts of meteorological variability on renewable energy production and power system modelling has been shown, as was also done in Ref. [17].

8. Conclusions and outlook

Given the societal importance of a secure and continuous energy supply, the meteorological sensitivity of a highly-renewable European power system was analysed. The main objective of this study was to investigate the meteorological situations that give rise to high risks related to European energy safety in a power system dependent on renewable energy production from wind and solar sources. Using large ensemble experiments from two global climate models (EC-Earth and HadGEM2-ES), 3×2000 years of daily energy yields and energy demand were calculated. From this data 1-in-10 year low renewable energy production events and 1-in-10 year high energy shortfall events of varying length (1-, 7-, and 14-days) were selected and investigated from

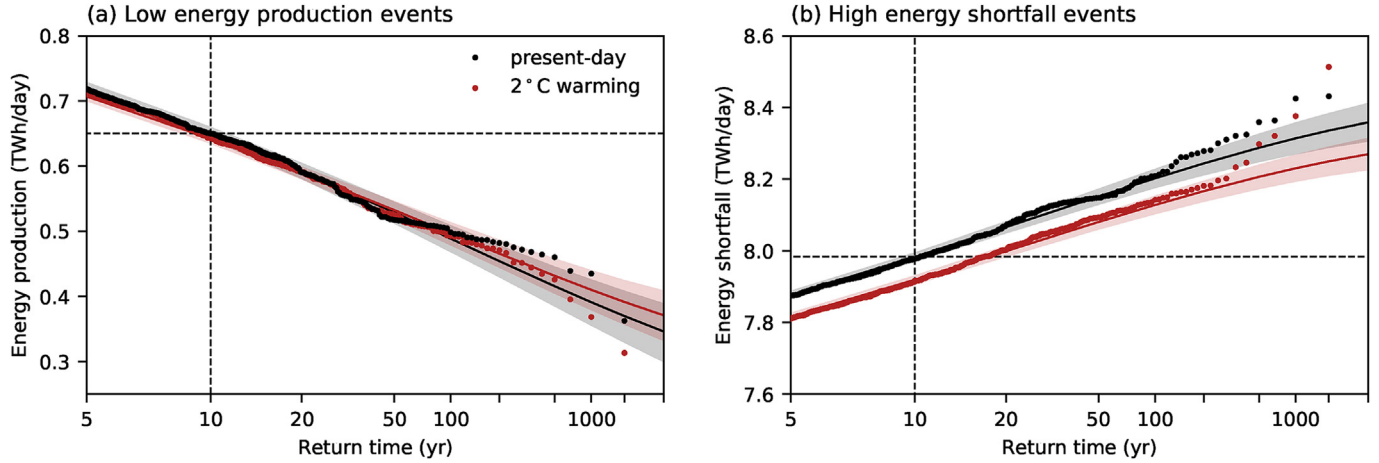

Fig. 14. Gumbel plots for (a) low energy production events, and (b) high energy shortfall events (TWh day^{-1}). Black colours show present-day conditions, red colours show projected pre-industrial + 2°C warming conditions, lines show a GEV fit, colour shading shows the 95% GEV confidence interval, the dashed black line indicates 1-in-10 year event threshold for present-day conditions.

a meteorological perspective. Energy shortfall was defined to be the difference between energy demand and renewable energy production.

1-day extreme low energy production events are characterised by a large high pressure system over central Europe, associated with lower than normal 10 m wind speeds all over Europe, but most pronounced over the North Sea and surrounding regions leading to low wind energy production. These events typically occur in the extended winter (October-February), therefore solar energy production is limited due to short day lengths. 1-day extreme high energy shortfall events are very similar (a high pressure system and negative wind anomalies), though now combined with colder than normal temperatures over the entire region. Electric heating requirements drive up energy demand. Low energy production combined with high energy demand leads to high energy shortfall. These energy shortfall events occur from November to March. The similarity between low energy production events and high energy shortfall events is high, 21% of the selected events are co-occurring, i.e. days are extreme (1-in-10 year return time) by both measures.

Atmospheric blocking can lead to prolonged episodes of large scale negative wind anomalies and cold temperatures. In these situations renewable energy production is low or energy shortfall is high for 7 or 14 days in a row. To guarantee a continuous energy supply, future European power systems with high penetrations of variable renewable energy must be designed with such events in mind. Longer lasting low energy production events tend to occur earlier in the year than 1-day low production events, this shift in the timing of events is not found for longer lasting energy shortfall events.

The described meteorological conditions leading to high impacts in the energy sector are consistent across two climate models. Similar extreme event analysis based on observational data is impossible due to the limited length of records. However, four 1-in-10 year events from ERA-interim data fall within the distribution of modelled events, providing confidence to the model results. The results are robust to changes in the spatial distribution of wind turbines and solar panels, these high pressure systems cover most of Europe and lower renewable energy production in the entire region. Options to import renewable energy from remote locations are therefore severely limited. The influence of continued global climate change is small compared to interannual variability.

The investigated extreme high energy shortfall events are key examples of compound events, i.e. a combination of multiple drivers and/or hazards that contribute to societal or environmental risk [63]. The selected 1-in-10 year high energy shortfall events are caused by 1-in-2.2 year low energy production combined with 1-in-0.3 year high energy demand. If one had assumed low energy production is the single driver for energy shortfall, associated risk estimates would have been severely underestimated: the selected 1-in-10 year low energy production events are just 1-in-1.9 year events in terms of high energy shortfall. An impact-based bottom-up approach, as used in this paper, is especially suitable to help identify driving mechanisms of risk in complex systems. The noted differences between low energy production events and high energy shortfall events, especially at longer timescales, shows that the precise method of event selection is important. Meteorological-focused studies (e.g. studies investigating a changing wind climate, changes in solar radiation or the change of occurrence of high pressure systems) provide understanding of single drivers, interactions between drivers are not considered (e.g. extreme low energy production may not lead to problems if energy demand is low as well, or increasing incoming radiation may increase solar energy production, though this may be offset by decreasing performance of solar cells due to rising temperatures). We therefore advocate for event selection based on impact variables as close as possible to the 'true' societal impact, and for more studies identifying interactions between climatic drivers, hazards and societal risk. Impact-based climate studies by interdisciplinary research teams provide a new way of analysing climate data and may help to build more resilient systems.

Acknowledgements

The authors would like to thank four reviewers for constructive comments and Kirien Whan for help with the GEV fits. This work is part of the HiWAVES3 project, funding was supplied by the Netherlands Organisation of Scientific Research (NWO): ALWCL.2016.2.

Appendix A. Supplementary material

Supplementary material related to this article can be found at https://doi.org/10.1016/j.rser.2019.04.065.

References

[1] Matthews HD, Gillett NP, Stott PA, Zickfeld K. The proportionality of global warming to cumulative carbon emissions. Nature 2009;459:829.
[2] Meinshausen M, Meinshausen N, Hare W, Raper SC, Frieler K, Knutti R, Frame DJ, Allen MR. Greenhouse-gas emission targets for limiting global warming to 2 °C. Nature 2009;458:1158.
[3] Armaroli N, Balzani V. Towards an electricity-powered world. Energy Environ Sci 2011;4:3193–222.
[4] Rogelj J, Schaeffer M, Meinshausen M, Knutti R, Alcamo J, Riahi K, Hare W. Zero emission targets as long-term global goals for climate protection. Environ Res Lett 2015;10:105007.
[5] Seneviratne SI, Donat MG, Pitman AJ, Knutti R, Wilby RL. Allowable CO2 emissions based on regional and impact-related climate targets. Nature 2016;529:477.
[6] Schleussner C-F, Lissner TK, Fischer EM, Wohland J, Perrette M, Golly A, Rogelj J, Childers K, Schewe J, Frieler K, et al. Differential climate impacts for policy-relevant limits to global warming: the case of 1.5 C and 2 C. Earth Syst. Dyn. 2016;7:327–51.
[7] Arnell NW, Lowe JA, Lloyd-Hughes B, Osborn TJ. The impacts avoided with a 1.5 °C climate target: a global and regional assessment. Clim Change 2018;147:61–76.
[8] Dosio A, Mentaschi L, Fischer EM, Wyser K. Extreme heat waves under 1.5 °C and 2 °C global warming. Environ Res Lett 2018;13. 054006.
[9] Rasmussen D, Bittermann K, Buchanan MK, Kulp S, Strauss BH, Kopp RE, Oppenheimer M. Extreme sea level implications of 1.5 °C, 2.0 °C, and 2.5 °C temperature stabilization targets in the 21st and 22nd centuries. Environ Res Lett 2018;13. 034040.
[10] Kavak Akpinar E, Akpinar S. An assessment on seasonal analysis of wind energy characteristics and wind turbine characteristics. Energy Convers Manag 2005;46:1848–67.
[11] Pryor SC, Barthelmie RJ, Schoof JT. Inter-annual variability of wind indices across Europe. Wind Energy: Int J Progress Appl Wind Power Convers Technol 2006;9:27–38.
[12] Šúri M, Huld TA, Dunlop ED, Ossenbrink HA. Potential of solar electricity generation in the European Union member states and candidate countries. Sol Energy 2007;81:1295–305.
[13] Roques F, Hiroux C, Saguan M. Optimal wind power deployment in Europea portfolio approach. Energy Policy 2010;38:3245–56.
[14] Davy RJ, Troccoli A. Interannual variability of solar energy generation in Australia. Sol Energy 2012;86:3554–60.
[15] Jerez S, Trigo RM, Vicente-Serrano SM, Pozo-Vázquez D, Lorente-Plazas R, Lorenzo-Lacruz J, Santos-Alamillos F, Montávez J. The impact of the North Atlantic Oscillation on renewable energy resources in southwestern Europe. J Appl Meteorol Climatol 2013;52:2204–25.
[16] Jerez S, Thais F, Tobin I, Wild M, Colette A, Yiou P, Vautard R. The CLIMIX model: a tool to create and evaluate spatially-resolved scenarios of photovoltaic and wind power development. Renew Sustain Energy Rev 2015;42:1–15.
[17] Bloomfield HC, Brayshaw DJ, Shaffrey LC, Coker PJ, Thornton HE. Quantifying the increasing sensitivity of power systems to climate variability. Environ Res Lett 2016;11:124025.
[18] Ravestein P, van der Schrier G, Haarsma R, Scheele R, van den Broek M. Vulnerability of European intermittent renewable energy supply to climate change and climate variability. Renew Sustain Energy Rev 2018;97:497–508.
[19] Sanchis G. Europes future secure and sustainable electricity infrastructure. Technical Report; 2015.
[20] Huber M, Dimkova D, Hamacher T. Integration of wind and solar power in Europe: assessment of flexibility requirements. Energy 2014;69:236–46.
[21] Sailor DJ. Relating residential and commercial sector electricity loads to climate evaluating state level sensitivities and vulnerabilities. Energy 2001;26:645–57.
[22] Valor E, Meneu V, Caselles V. Daily air temperature and electricity load in Spain. J Appl Meteorol 2001;40:1413–21.
[23] Bessec M, Fouquau J. The non-linear link between electricity consumption and temperature in Europe: a threshold panel approach. Energy Econ 2008;30:2705–21.
[24] Isaac M, Van Vuuren DP. Modeling global residential sector energy demand for heating and air conditioning in the context of climate change. Energy Policy 2009;37:507–21.
[25] Bloomfield HC, Brayshaw DJ, Shaffrey LC, Coker PJ, Thornton HE. The changing sensitivity of power systems to meteorological drivers: a case study of Great Britain. Environ Res Lett 2018;13. 054028.
[26] Staffell I, Pfenninger S. The increasing impact of weather on electricity supply and demand. Energy 2018;145:65–78.

[27] Giebel G. Equalizing Effects of the Wind Energy Production in Northern Europe Determined from Reanalysis Data, Roskilde, Risoe 20. 2000.
[28] Grams CM, Beerli R, Pfenninger S, Staffell I, Wernli H. Balancing Europes wind-power output through spatial deployment informed by weather regimes. Nat Clim Change 2017;7:557.
[29] Hazeleger W, Wang X, Severijns C, Ştefănescu S, Bintanja R, Sterl A, Wyser K, Semmler T, Yang S, Van den Hurk B, van Noije T, van der Linden E, van der Wiel K. EC-Earth V2.2: description and validation of a new seamless Earth system prediction model. Clim Dyn 2012;39:2611–29.
[30] Morice CP, Kennedy JJ, Rayner NA, Jones PD. Quantifying uncertainties in global and regional temperature change using an ensemble of observational estimates: the HadCRUT4 data set. J Geophys Res: Atmosphere 2012;117.
[31] van der Wiel K, Wanders N, Selten FM, Bierkens MFP. Added value of large ensemble simulations for assessing extreme river discharge in a 2 °C warmer world. Geophys Res Lett 2019;46:2093–102.
[32] Dee DP, Uppala SM, Simmons A, Berrisford P, Poli P, Kobayashi S, Andrae U, Balmaseda M, Balsamo G, Bauer d P, et al. The ERA-Interim reanalysis: configuration and performance of the data assimilation system. Q J R Meteorol Soc 2011;137:553–97.
[33] Martin GM, Bellouin N, Collins W, Culverwell I, Halloran P, Hardiman S, Hinton T, Jones C, McDonald R, McLaren A, O'Connor F, et al. The HadGEM2 family of met office unified model climate configurations. Geosci Model Dev (GMD) 2011;4:723–57.
[34] UNFCCC. Adoption of the Paris agreement Report No FCCC/CP/2015/L.9/Rev.1 2015.
[35] CIESIN. Gridded population of the world, version 4 (GPWv4): population density, palisades, NY: NASA socioeconomic data and applications center (SEDAC). 2016. Version: November 2017 release.
[36] Hsu S, Meindl EA, Gilhousen DB. Determining the power-law wind-profile exponent under near-neutral stability conditions at sea. J Appl Meteorol 1994;33:757–65.
[37] Mathew S. Wind energy: fundamentals, resource analysis and economics. Berlin Heidelberg: Springer; 2007.
[38] Carrillo C, Montaño AO, Cidrás J, Díaz-Dorado E. Review of power curve modelling for wind turbines. Renew Sustain Energy Rev 2013;21:572–81.
[39] Chenni R, Makhlouf M, Kerbache T, Bouzid A. A detailed modeling method for photovoltaic cells. Energy 2007;32:1724–30.
[40] TamizhMani G, Ji L, Tang Y, Petacci L, Osterwald C. Photovoltaic module thermal/wind performance: long-term monitoring and model development for energy rating. NCPV and solar program review meeting, volume 2003. NREL; 2003.
[41] Forsythe WC, Rykiel Jr. EJ, Stahl RS, Wu H-i, Schoolfield RM. A model comparison for daylength as a function of latitude and day of year. Ecol Model 1995;80:87–95.
[42] Teräsvirta T. Specification, estimation, and evaluation of smooth transition autoregressive models. J Am Stat Assoc 1994;89:208–18.
[43] Moral-Carcedo J, Vicens-Otero J. Modelling the non-linear response of Spanish electricity demand to temperature variations. Energy Econ 2005;27:477–94.
[44] Woollings T, Barriopedro D, Methven J, Son S-W, Martius O, Harvey B, Sillmann J, Lupo AR, Seneviratne S. Blocking and its Response to Climate Change, Current Climate Change Reports 4. 2018. p. 287–300.
[45] Pryor SC, Barthelmie RJ, Kjellström E. Potential climate change impact on wind energy resources in northern Europe: analyses using a regional climate model. Clim Dyn 2005;25:815–35.
[46] Pryor SC, Barthelmie RJ. Climate change impacts on wind energy: a review. Renew Sustain Energy Rev 2010;14:430–7.
[47] Hueging H, Haas R, Born K, Jacob D, Pinto JG. Regional changes in wind energy potential over Europe using regional climate model ensemble projections. J Appl Meteorol Climatol 2013;52:903–17.
[48] Reyers M, Moemken J, Pinto JG. Future changes of wind energy potentials over Europe in a large CMIP5 multi-model ensemble. Int J Climatol 2016;36:783–96.
[49] Davy R, Gnatiuk N, Pettersson L, Bobylev L. Climate change impacts on wind energy potential in the European domain with a focus on the black sea. Renewable and Sustainable Energy Reviews; 2017.
[50] Jerez S, Tobin I, Vautard R, Montávez JP, López-Romero JM, Thais F, Bartok B, Christensen OB, Colette A, Déqué M, et al. The impact of climate change on photovoltaic power generation in Europe. Nat Commun 2015;6:10014.
[51] Wild M, Folini D, Henschel F, Fischer N, Müller B. Projections of long-term changes in solar radiation based on CMIP5 climate models and their influence on energy yields of photovoltaic systems. Sol Energy 2015;116:12–24.
[52] De Cian E, Lanzi E, Roson R. Seasonal temperature variations and energy demand. Clim Change 2013;116:805–25.
[53] De Cian E, Wing IS. Global energy consumption in a warming climate. Environ Resour Econ 2017:1–46.
[54] Gilleland E, Katz RW, et al. extRemes 2.0: an extreme value analysis package in R. J Stat Softw 2016;72:1–39.
[55] IPCC. Stocker TF, Qin D, Plattner G-K, Tignor M, Allen SK, Boschung J, Nauels A, Xia Y, Bex V, Midgley PM, editors. Climate change 2013: the physical science basis. Contribution of working group I to the fifth assessment report of the intergovernmental panel on climate change Cambridge, UK and New York, NY, USA: Cambridge University Press; 2013. https://doi.org/10.1017/CBO9781107415324.
[56] Pryor SC, Nikulin G, Jones C. Influence of spatial resolution on regional climate model derived wind climates. J Geophys Res: Atmosphere 2012;117.
[57] Kalverla PC, Steeneveld G-J, Ronda RJ, Holtslag AA. An observational climatology of anomalous wind events at offshore meteomast IJmuiden (North Sea). J Wind Eng Ind Aerodyn 2017;165:86–99.
[58] Berckmans J, Woollings T, Demory M-E, Vidale P-L, Roberts M. Atmospheric blocking in a high resolution climate model: influences of mean state, orography and eddy forcing. Atmos Sci Lett 2013;14:34–40.
[59] Amato AD, Ruth M, Kirshen P, Horwitz J. Regional energy demand responses to climate change: methodology and application to the commonwealth of Massachusetts. Clim Change 2005;71:175–201.
[60] Tobin I, Jerez S, Vautard R, Thais F, Van Meijgaard E, Prein A, Déqué M, Kotlarski S, Maule CF, Nikulin G, et al. Climate change impacts on the power generation potential of a European mid-century wind farms scenario. Environ Res Lett 2016;11. 034013.
[61] Pozo-Vázquez D, Tovar-Pescador J, Gámiz-Fortis S, Esteban-Parra M, Castro-Díez Y. NAO and solar radiation variability in the European North Atlantic region. Geophys Res Lett 2004;31.
[62] Clark RT, Bett PE, Thornton HE, Scaife AA. Skilful seasonal predictions for the European energy industry. Environ Res Lett 2017;12. 024002.
[63] Zscheischler J, Westra S, Hurk BJ, Seneviratne SI, Ward PJ, Pitman A, AghaKouchak A, Bresch DN, Leonard M, Wahl T, et al. Future climate risk from compound events. Nat Clim Change 2018:1.